Fully nonlinear three-dimensional convection in a rapidly rotating layer

Keith Julien
Department of Applied Mathematics, University of Colorado, Boulder, Colorado 80309

Edgar Knobloch
Department of Physics, University of California, Berkeley, California 94720

(Received 9 June 1998; accepted 16 February 1999)

Fully nonlinear three-dimensional convection in a rotating layer is studied for large Taylor numbers. In this regime, the leading order nonlinearity arises from the distortion of the horizontally averaged temperature profile. As a result, steady rolls, squares, hexagons, triangles, and a pattern called patchwork quilt all have identical Nusselt numbers. A similar degeneracy is present in overstable convection with six patterns having identical time-averaged Nusselt numbers and oscillation frequencies. These results are obtained via an asymptotic expansion in the Taylor number that determines, for each Rayleigh number, the time-averaged Nusselt number and oscillation frequency from the solution of a nonlinear eigenvalue problem for the vertical temperature profile. A number of other patterns are determined by a weakly nonlinear analysis that cannot be extended into the fully nonlinear regime by the present methods, but these patterns are necessarily unstable. © *1999 American Institute of Physics.* [S1070-6631(99)01606-2]

I. INTRODUCTION

Square pattern convection in a rotating layer is featured prominently on the cover of the Dover edition of Chandrasekhar's famous book.[1] This figure, reproduced from original work by Veronis,[2] shows particle trajectories in (steady) square pattern convection at onset, i.e., the streamlines of the linear eigenfunction. At slightly supercritical forcing ($\mathrm{Ra}=\mathrm{Ra}_c+\epsilon^2$, where Ra is the Rayleigh number and $\epsilon \ll 1$), the velocity field resembles the linear eigenfunction and the particle paths might be expected to resemble those depicted on the cover of the book.[3] The computed streamline pattern is periodic in the plane and has a pronounced Z_4 symmetry, i.e., it is invariant under proper rotations by $\pi/2$ only. In this paper we show, following Bassom and Zhang,[4] that fully nonlinear velocity fields with Z_4 symmetry can be obtained in the limit of large rotation rates by combining asymptotic analysis of the governing partial differential equations with a numerical solution of a nonlinear eigenvalue problem for the heat flux. The resulting solutions are valid at Rayleigh numbers arbitrarily far above threshold, in contrast to the weakly nonlinear solutions obtainable via perturbation theory when $\mathrm{Ra}=\mathrm{Ra}_c+\epsilon^2$, $\epsilon \ll 1$. However, despite this fact, their horizontal structure remains simple: the nonlinearity manifests itself only in their vertical structure. Fundamentally, this is because in the rapid rotation limit the dominant Coriolis term is balanced, at leading order, by the pressure gradient. As a result, the leading order description involves nonlinearities from the temperature equation only. We describe here the asymptotic expansion leading to these conclusions and generalize it to both overstable convection with a square planform and to other planforms. A number of additional results are easily obtained in this limit. These include results on several other types of patterns which can only be found by perturbation methods valid near onset. This is the case, for example, for an oscillatory pattern called alternating rolls; this pattern bifurcates supercritically but is always unstable near onset. Although these results are formally obtained for stress-free boundary conditions, in the rapid rotation limit they are identical to those for no-slip boundary conditions.

This paper is organized as follows. In the next section we introduce the governing equations and summarize their linear stability properties. In Sec. III we describe the asymptotic expansion that leads to a new class of reduced equations describing fully nonlinear convection in the rapid rotation limit. These equations take the form of coupled equations for the vertical velocity and vertical vorticity, driven by thermal buoyancy, and describe the dynamics outside of the thin Ekman boundary layers at the top and bottom. As a result they form a simplified set of equations governing the three-dimensional dynamics in a rapidly rotating layer at arbitrary Rayleigh numbers. Although these equations are of interest in their own right,[5] we focus here on spatially periodic solutions only. In Sec. IV we describe steady and oscillatory solutions with a square planform, turning in Sec. V to other types of steady and oscillatory patterns. In Sec. VI we summarize the results of solving the nonlinear eigenvalue problems that arise at high Rayleigh numbers. The paper ends with a discussion of the implications of the fully nonlinear three-dimensional solutions constructed here for ongoing simulations of turbulent rotating convection.[6]

II. GOVERNING EQUATIONS

The dimensionless Boussinesq equations describing convection in a horizontal fluid layer rotating uniformly about the vertical are[1]

$$\frac{1}{\sigma}\frac{D\mathbf{u}}{Dt}+Ta^{1/2}\hat{\mathbf{z}}\times\mathbf{u}=-\nabla p+\mathrm{Ra}\,T\hat{\mathbf{z}}+\nabla^2\mathbf{u}, \tag{1}$$

$$\frac{DT}{Dt}=\nabla^2 T, \tag{2}$$

$$\nabla\cdot\mathbf{u}=0, \tag{3}$$

where $\mathbf{u}=(u,v,w)$ is the velocity field in Cartesian coordinates (x,y,z) with z vertically upward. The symbols T and p denote the temperature and pressure, respectively. The equations have been nondimensionalized with respect to the thermal diffusion time in the vertical. The resulting dimensionless parameters

$$\mathrm{Ta}=\frac{4\Omega^2 d^4}{\nu^2},\quad \mathrm{Ra}=\frac{g\alpha\Delta T d^3}{\nu\kappa},\quad \sigma=\frac{\nu}{\kappa}, \tag{4}$$

are the Taylor, Rayleigh, and Prandtl numbers, and measure the magnitude of the rotation rate Ω, the strength of the applied buoyancy force, and the ratio of viscous and thermal diffusion times. Here d is the layer depth, and ν and κ are, respectively, the kinematic viscosity and thermal diffusivity. Of the remaining symbols, ΔT is the temperature difference imposed across the layer while g is the acceleration due to gravity and α the coefficient of thermal expansion.

In the following we employ a stream function formulation in order to avoid difficulties in imposing the incompressibility requirement (3) on the velocity field at each order in the asymptotic expansion. Specifically, we write

$$\mathbf{u}=\nabla\times\phi\hat{\mathbf{z}}+\nabla\times\nabla\times\psi\hat{\mathbf{z}}, \tag{5}$$

so that

$$\mathbf{u}=\begin{pmatrix} \partial_y\phi & + & \partial_x\partial_z\psi \\ -\partial_x\phi & + & \partial_y\partial_z\psi \\ & - & \nabla_\perp^2\psi \end{pmatrix},$$

$$\omega=\begin{pmatrix} \partial_x\partial_z\phi & - & \nabla^2\partial_y\psi \\ \partial_y\partial_z\phi & + & \nabla^2\partial_x\psi \\ & - & \nabla_\perp^2\phi \end{pmatrix}. \tag{6}$$

Here $\omega\equiv\nabla\times\mathbf{u}$ is the vorticity and the partials with subscripts denote differentiation: $\partial_x\equiv\partial/\partial x$, etc. The operator $\nabla_\perp^2\equiv\partial_{xx}+\partial_{yy}$ is the horizontal Laplacian.

In the following we shall find it convenient to introduce the Ekman number, $E=Ta^{-1/2}$, as a measure of the importance of dissipation compared with rotation, and rescale the equations with $t\sim Et'$, $\mathbf{u}\sim E^{-1}\mathbf{u}'$. Dropping primes, and taking $\hat{\mathbf{z}}\cdot\nabla\times$ and $\hat{\mathbf{z}}\cdot\nabla\times\nabla\times$ of the momentum equation, puts the governing equations into the form

$$\frac{1}{\sigma}\partial_t\nabla_\perp^2\phi-\partial_z\nabla_\perp^2\psi+\frac{1}{\sigma}N_\phi(\phi,\psi)=E\nabla^2\nabla_\perp^2\phi, \tag{7}$$

$$\frac{1}{\sigma}\partial_t\nabla^2\nabla_\perp^2\psi+\partial_z\nabla_\perp^2\phi+\frac{1}{\sigma}N_\psi(\phi,\psi)$$
$$=-\mathrm{Ra}\,E^2\nabla_\perp^2 T+E\nabla^4\nabla_\perp^2\psi, \tag{8}$$

$$\partial_t T+N_T(\phi,\psi,T)=E\nabla^2 T, \tag{9}$$

where

$$N_\phi(\phi,\psi)=(\omega\cdot\nabla)w-(\mathbf{u}\cdot\nabla)\omega_3,$$
$$N_\psi(\phi,\psi)=\hat{\mathbf{z}}\cdot\nabla\times\nabla\times(\omega\times\mathbf{u}), \tag{10}$$
$$N_T(\phi,\psi,T)=\mathbf{u}\cdot\nabla T.$$

In the streamfunction representation these terms take the form

$$N_\phi=-J[\phi,\nabla_\perp^2\phi]-J[\nabla^2\psi,\nabla_\perp^2\psi]+\nabla_\perp(\nabla_\perp^2\phi)\cdot\nabla_\perp(\partial_z\psi)$$
$$-\nabla_\perp(\partial_z\phi)\cdot\nabla_\perp(\nabla_\perp^2\psi)-\nabla_\perp^2\psi\nabla_\perp^2(\partial_z\phi)$$
$$+\nabla_\perp^2\phi\nabla_\perp^2(\partial_z\psi),$$

$$N_\psi=-\nabla^2\{J[\phi,\nabla^2\psi]+J[\partial_z\phi,\partial_z\psi]-\nabla_\perp\phi\cdot\nabla_\perp(\partial_z\phi)-\nabla_\perp(\partial_z\psi)\cdot\nabla_\perp(\nabla^2\psi)\}-\partial_z\{J[\partial_z\psi,\nabla^2\phi]-J[\phi,\nabla^2\partial_z\psi]$$
$$-2J[\partial_z\phi,\nabla^2\psi]+\nabla_\perp\phi\cdot\nabla_\perp(\nabla^2\phi)+\nabla_\perp(\partial_z\psi)\cdot\nabla_\perp(\nabla^2\partial_z\psi)+\nabla_\perp^2\psi\nabla^2(\nabla_\perp^2\psi)+|\nabla_\perp(\partial_z\phi)|^2+|\nabla_\perp(\nabla^2\psi)|^2+(\nabla_\perp^2\phi)^2\},$$
$$N_T=-J[\phi,T]+\nabla_\perp\partial_z\psi\cdot\nabla_\perp T-\nabla_\perp^2\psi\partial_z T, \tag{11}$$

where $J[\cdot,\cdot]$ denotes the horizontal Jacobian $\partial_x\cdot\partial_y\cdot-\partial_y\cdot\partial_x\cdot$. These equations are solved for a fluid confined between boundaries at fixed temperatures,

$$T(0)=1,\quad T(1)=0, \tag{12}$$

which are impenetrable and either stress-free or no-slip,

$$\text{stress-free:}\quad \psi=\partial_{zz}\psi=\partial_z\phi=0\quad \text{at } z=0,1,$$
$$\text{no-slip:}\quad \psi=\partial_z\psi=\phi=0\quad \text{at } z=0,1. \tag{13}$$

The stability properties of the conduction state

$$\psi=\phi=0,\quad T=1-z, \tag{14}$$

are summarized in Ref. 1 (see also Ref. 7). In the rapid rotation limit these results become independent of the nature of the velocity boundary conditions at the top and bottom of the layer.[8] In this limit one finds that for $\sigma>\sigma^*\approx 0.676\,605$ the conduction state loses stability at a steady-state bifurcation at

$$\mathrm{Ra}_c^{(s)}=3\left[\frac{\pi^2}{2}\right]^{2/3}E^{-4/3},\quad k_c^{(s)}=\left[\frac{\pi^2}{2}\right]^{1/6}E^{-1/3}, \tag{15}$$

while for $\sigma<\sigma^*$ (see Fig. 1) it loses stability to overstable oscillations (Hopf bifurcation) at

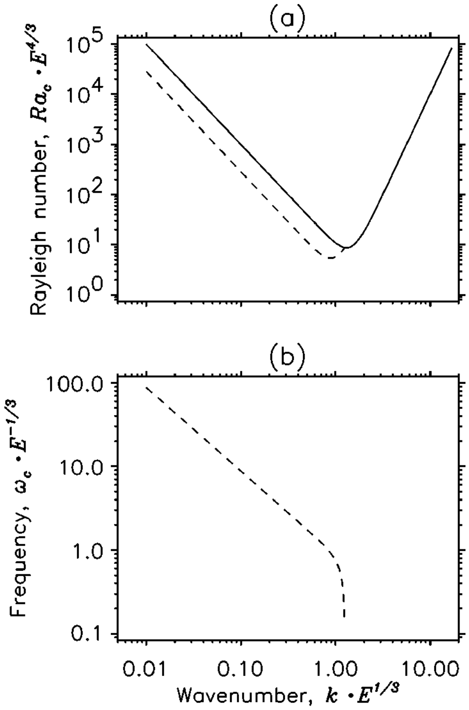

FIG. 1. (a) Neutral stability curves $\mathrm{Ra}_c(k)$ for steady (solid line) and oscillatory (dashed line) convection when $\sigma=0.4574$; the minimum of the dashed curve defines $k_c^{(o)}=0.8867$, $\mathrm{Ra}_c^{(o)}=5.4059$. The Takens–Bogdanov point occurs at $k_{\mathrm{TB}}=1.2422$, $\mathrm{Ra}_{TB}=8.7771$. (b) The corresponding oscillation frequency ω_c vanishes at k_{TB}.

$$\mathrm{Ra}_c^{(o)}=3\left[\frac{2}{1+\sigma}\right]^{1/3}(\sigma\pi)^{4/3}E^{-4/3}, \tag{16}$$

with

$$k_c^{(o)}=\left[\frac{\sigma^2\pi^2}{2(1+\sigma)^2}\right]^{1/6}E^{-1/3},$$
$$\omega_c^{(o)}=\left[\frac{\sigma^2\pi^2}{2(1+\sigma)^2}\right]^{1/3}(2-3\sigma^2)^{1/2}E^{1/3}. \tag{17}$$

Here $\omega_c^{(o)}$ is the Hopf frequency in the new time variable.

III. THE SCALED EQUATIONS

In the following we focus on horizontal scales of order $E^{1/3}d$; as indicated above, scales of this order are the ones selected by linear stability theory. We therefore introduce fast horizontal variables $x'\equiv E^{-1/3}x$, $y'\equiv E^{-1/3}y$ and use the notation $D\equiv\partial_z$ to denote derivatives with respect to the (slow) variable z. Since the motion on the horizontal scales will be in geostrophic balance we also introduce a slow time $t'\equiv E^{1/3}t$,

$$\partial_x,\partial_y=E^{-1/3}(\partial_{x'},\partial_{y'}), \quad \partial_t=E^{1/3}\partial_{t'}. \tag{18}$$

Similar anisotropic scalings have been observed both in numerical simulations and laboratory experiments.[6,9,10] Next, to introduce nonlinearity in the leading order balance we scale the streamfunctions as

$$\phi=E\phi', \quad \psi=E^{4/3}\psi', \tag{19}$$

and write

$$T(x,y,z,t)=\overline{T}(z)+E^{1/3}\theta(x,y,z,t)+\mathcal{O}(E^{2/3}). \tag{20}$$

Here the overbar indicates averaging over both the horizontal variables x,y and over time t. In the following we shall only be interested in solutions that are periodic with respect to these three variables. Finally, according to (15) and (16), we also scale the Rayleigh number, $\mathrm{Ra}=E^{-4/3}\,\mathrm{Ra}'$.

The scalings (18) and (19) imply that on the scales of interest the vertical and horizontal velocities are of the same order, both $\mathcal{O}(E^{2/3})\Omega d$ in dimensional units. The local Rossby number is thus $\mathcal{O}(E^{1/3})$ and hence is small, i.e., even though the scales of interest are small the flow is still rotation-dominated. Moreover, as can be verified from Eq. (6), the horizontal velocity components are in geostrophic balance at leading order. Applying these scalings to Eqs. (7) and (8) (and dropping all primes) leads to the following reduced system:

$$\frac{1}{\sigma}[\partial_t\nabla_\perp^2\phi-J(\phi,\nabla_\perp^2\phi)]-D\nabla_\perp^2\psi=\nabla_\perp^4\phi+\mathcal{O}(E^{1/3}), \tag{21}$$

$$\frac{1}{\sigma}[\partial_t\nabla_\perp^2\psi-J(\phi,\nabla_\perp^2\psi)]+D\phi=-\mathrm{Ra}\,\theta+\nabla_\perp^4\psi+\mathcal{O}(E^{1/3}). \tag{22}$$

These equations represent a pair of coupled, thermally forced equations for the vertical velocity $w\equiv-\nabla_\perp^2\psi$ and the vertical vorticity $\zeta\equiv-\nabla_\perp^2\phi$. The thermal forcing follows from the temperature equation, which yields a pair of equations, one describing the evolution of the fluctuating temperature θ and the other a steady-state equation for the mean temperature profile $\overline{T}$,

$$\partial_t\theta-J(\phi,\theta)-\nabla_\perp^2\psi D\overline{T}=\nabla_\perp^2\theta+\mathcal{O}(E^{1/3}), \tag{23}$$

$$D^2\overline{T}+D\overline{\nabla_\perp^2\psi\theta}=\mathcal{O}(E^{1/3}). \tag{24}$$

To obtain these equations we have employed integration by parts assuming that u, v, and θ are periodic in space and time. Equation (24) can be readily integrated to obtain

$$D\overline{T}+\overline{\nabla_\perp^2\psi\theta}=-K, \tag{25}$$

where K is a constant determined by the temperature boundary conditions (12). Physically, K is the time-averaged Nusselt number, i.e., the total dimensionless heat flux (conductive and convective) across the layer. Equations (21)–(24) form a closed system of equations describing nonlinear convection in the rapid rotation limit.

It is important to observe that Eqs. (21)–(24) have an extra symmetry that is not present in the original Eqs. (1)–(3). This is the reflection

$$(x,y)\rightarrow(x,-y), \quad (\psi,\phi,\theta,\overline{T})\rightarrow(-\psi,-\phi,-\theta,\overline{T}). \tag{26}$$

Physically, this extra symmetry manifests itself in the absence of pseudoscalar terms in (21)–(24). In fact, we have the remarkable result that the symmetry properties of rotating convection in the rapid rotation limit are identical to those characteristic of nonrotating convection! It is not surprising, therefore, that the presence of this ''unexpected'' symmetry has important consequences for the types of solutions admitted by these equations and for their stability. It should be noted, however, that the (scaled) horizontal velocity components,

$$(u,v)=(\partial_y\phi+E^{1/3}\partial_x\partial_z\psi,-\partial_x\phi+E^{1/3}\partial_y\partial_z\psi), \tag{27}$$

do not share this symmetry. In fact, the velocity components are symmetric with respect to (26) only at leading order in the Taylor number, i.e., $(u,v)\to(u,-v)$ only if the subdominant ψ terms in (27) are omitted. Such terms are, however, essential in order to satisfy the incompressibility condition (3). Thus at any finite (but nonzero) Taylor number the flow will manifest the handedness expected of rotating flows and the symmetries of the Navier–Stokes equation in its primitive variable representation.

In the following we focus on solutions of Eqs. (21)–(24) that are periodic in space and time. It turns out that many of these have horizontal structure that remains simple for all values of Ra. In the next section we describe solutions with a square planform that have this property and then generalize the results to other planforms. Turbulent solutions of (21)–(24) are discussed elsewhere.[5]

IV. SOLUTIONS WITH A SQUARE PLANFORM

A. Weakly nonlinear theory

For patterns with a square planform the general theory[11,12] is conveniently formulated on a rotating square lattice. In the steady case, the resulting weakly nonlinear theory identifies two competing patterns that are periodic on this lattice and bifurcate simultaneously from the conduction state:[11] rolls (R) and squares (S). Because of the rotation the square pattern has Z_4 symmetry, i.e., it is invariant under proper rotations by $\pi/2$ only, cf. Ref. 1. In the case of overstability, four solutions with the symmetry of a rotating square lattice bifurcate simultaneously from the conduction state:[12] traveling rolls (TR), standing rolls (SR), standing squares (SS), and alternating rolls (AR). In each case the stability of these solutions with respect to perturbations in the form of the competing solutions can be calculated. For steady rotating convection such calculations are described in Ref. 11. Analogous calculations for the overstable problem have not been done, although the abstract results are given in Ref. 12. In the following we show that with the exception of AR, fully nonlinear solutions of the above types can be found in the limit of large Taylor numbers, and calculate the AR state at small amplitude. We also find an unexpected solution, traveling squares (TS), and trace its presence to the unexpected symmetry (26).

To indicate the nature of these solutions we briefly recapitulate the abstract theory. In the case of steady onset we look for solutions of the form

$$\psi(x,y,z)=\tfrac{1}{2}\{A_1e^{ikx}+A_2e^{iky}\}f(z)+\cdots+\text{c.c.}, \tag{28}$$

where $f(z)$ is the vertical eigenfunction and the dots denote higher order terms in the bifurcation parameter $\lambda \equiv(\mathrm{Ra}-\mathrm{Ra}_c^{(s)})/\mathrm{Ra}_c^{(s)}$ whose amplitudes are slaved to the evolution of the amplitudes A_1,A_2. In equilibrium these amplitudes satisfy the equations

$$\begin{aligned}&(\mu(\lambda)+a|A_1|^2+b|A_2|^2)A_1=0,\\&(\mu(\lambda)+a|A_2|^2+b|A_1|^2)A_2=0,\end{aligned} \tag{29}$$

where $\mu'(0)>0$ and a,b are real coefficients. Generically these equations have two types of solutions, rolls and squares, given by $(A_1,A_2)=(A,0)$, and $(A_1,A_2)=(A,A)$, respectively. In the case of overstability we look analogously for solutions of the form

$$\begin{aligned}\psi(x,y,z,t)=\tfrac{1}{2}\{&A_1(t)e^{ikx}+A_2(t)e^{iky}+A_3(t)e^{-ikx}\\&+A_4(t)e^{-iky}\}f(z)+\cdots+\text{c.c.},\end{aligned} \tag{30}$$

and assume that the linear stability problem takes the form $\dot{\mathbf{A}}=\mu(\lambda)\mathbf{A}$, where $\mathbf{A}\equiv(A_1,A_2,A_3,A_4)$, $\lambda\equiv(\mathrm{Ra}-\mathrm{Ra}_c^{(o)})/\mathrm{Ra}_c^{(o)}$ and $\mu(0)=i\omega_c^{(o)}$, $\mathrm{Re}(\mu'(0))>0$. It follows that the quantities $(|A_1|,|A_3|)$ and $(|A_2|,|A_4|)$ represent amplitudes of left- and right-traveling waves in the x,y directions, respectively. In the generic $Z_4\times T^2$-symmetric problem the amplitudes A_j, $j=1,...,4$, satisfy the truncated equations[12,13]

$$\begin{aligned}\dot{A}_1&=\mu(\lambda)A_1+(a|A_1|^2+b|A_3|^2+c|A_2|^2+d|A_4|^2)A_1\\&\quad+eA_2A_4\bar{A}_3,\\\dot{A}_2&=\mu(\lambda)A_2+(a|A_2|^2+b|A_4|^2+c|A_3|^2+d|A_1|^2)A_2\\&\quad+eA_1A_3\bar{A}_4,\\\dot{A}_3&=\mu(\lambda)A_3+(a|A_3|^2+b|A_1|^2+c|A_4|^2+d|A_2|^2)A_3\\&\quad+eA_2A_4\bar{A}_1,\\\dot{A}_4&=\mu(\lambda)A_4+(a|A_4|^2+b|A_2|^2+c|A_1|^2+d|A_3|^2)A_4\\&\quad+eA_1A_3\bar{A}_2.\end{aligned} \tag{31}$$

However, in the present case the reflection symmetry (26) forces the coefficients c and d to be identical. This is because it acts on the complex amplitudes (A_1,A_2,A_3,A_4) by

$$(A_1,A_2,A_3,A_4)\to(A_1,-A_4,A_3,-A_2). \tag{32}$$

As a result, in the rapid rotation limit, the symmetry group becomes $D_4\times T^2$ instead of the expected symmetry $Z_4\times T^2$. The behavior of the resulting equations is analyzed in Ref. 14 and differs substantially from the generic case studied in Ref. 15.

It follows that the small amplitude temporally periodic solutions created at the Hopf bifurcation satisfy the equation $\dot{\mathbf{A}}=i(\omega-\omega_c^{(o)})\mathbf{A}$, where

$$\begin{aligned}&\nu A_1+(a|A_1|^2+b|A_3|^2+c|A_2|^2+c|A_4|^2)A_1+eA_2A_4\bar{A}_3=0,\\&\nu A_2+(a|A_2|^2+b|A_4|^2+c|A_3|^2+c|A_1|^2)A_2+eA_1A_3\bar{A}_4=0,\\&\nu A_3+(a|A_3|^2+b|A_1|^2+c|A_4|^2+c|A_2|^2)A_3+eA_2A_4\bar{A}_1=0,\\&\nu A_4+(a|A_4|^2+b|A_2|^2+c|A_1|^2+c|A_3|^2)A_4+eA_1A_3\bar{A}_2=0,\end{aligned} \tag{33}$$

where $\nu=\mu(\lambda)-i(\omega-\omega_c^{(o)})$, and the frequency $\omega\approx\omega_c^{(o)}$ is to be determined. The coefficients μ, a, b, c and e are in general all complex.

The following five solutions are guaranteed to be present near onset of overstability.[14]

$$
\begin{aligned}
&\text{Traveling Rolls (TR):} \quad (A,0,0,0),\\
&\text{Standing Rolls (SR):} \quad (A,0,A,0),\\
&\text{Standing Squares (SS):} \quad (A,A,A,A),\\
&\text{Alternating Rolls (AR):} \quad (A,iA,A,iA),\\
&\text{Traveling Squares (TS):} \quad (A,A,0,0).
\end{aligned}
\tag{34}
$$

A sixth pattern, called standing cross-rolls (SCR), exists in open regions in coefficient space, but is always unstable. It will not be considered here. Note that in the generic $Z_4\times T^2$-symmetric case in which $c\neq d$, traveling squares cease to be a primary solution branch;[12] instead, the analog of TS bifurcates in a secondary bifurcation from one of the other branches which persist as primary branches even when $c\neq d$.

The predictions of the weakly nonlinear theory are expected to hold even for fully nonlinear convection. However, as shown below, we can find fully nonlinear solutions in the form of TR, SR, and SS only; the remaining two sets of solutions can be determined analytically in the weakly nonlinear regime only. For the fully nonlinear solutions we find, by continuation arguments, that if the solution frequency remains bounded away from zero the branches exist globally. Moreover, if such a branch is stable near onset it can lose stability only at a secondary saddle-node bifurcation, at a secondary Hopf bifurcation, or at a parity-breaking bifurcation. If the amplitude increases monotonically with Ra, no saddle-node bifurcations are present. A secondary Hopf bifurcation from the TR branch generates a branch of two-frequency modulated waves which may terminate on one of the other branches in a parity-breaking bifurcation.[16] Hopf bifurcations from SR and SS may take the form of two-frequency standing waves or three-frequency standing waves that drift back and forth.[17] Parity-breaking bifurcations are steady-state bifurcations from a group orbit of nondrifting solutions that result in a drift. Such drifting standing waves are two-frequency states and often connect with the two-frequency waves generated by secondary Hopf bifurcations from traveling states. None of these bifurcations can be found without an explicit stability calculation. Additional wavelength changing instabilities are also possible, but require the use of periodic boundary conditions based on multiple wavelengths of the basic state. We do not pursue these possibilities here.

B. Fully nonlinear solutions

The preceding section tells us what patterns we should expect in the fully nonlinear regime. We begin by looking for solutions with a square planform,

$$
\begin{aligned}
(\psi,\phi,\theta)=\tfrac{1}{2}(A(z),B(z),C(z))e^{i\omega t}\{e^{ikx}+e^{iky}\\
+e^{-ikx}+e^{-iky}\}+\text{c.c.}+\mathcal{O}(E^{1/3}).
\end{aligned}
\tag{35}
$$

Both steady ($\omega=0$) and oscillatory ($\omega\neq0$) patterns take this form. In the following we refer to $|A|$ as the amplitude of the solution. For this planform the Jacobians $J(\phi,\nabla_\perp^2\phi)$, $J(\phi,\nabla_\perp^2\psi)$, and $J(\phi,\theta)$ all vanish. It follows from Eqs. (21)–(23) that

$$
\begin{aligned}
&\left(\frac{i\omega}{\sigma}+k^2\right)B=DA, \quad k^2\left(\frac{i\omega}{\sigma}+k^2\right)A-\text{Ra}\,C=DB,\\
&(i\omega+k^2)C=-k^2AD\overline{T}.
\end{aligned}
\tag{36}
$$

The mean temperature Eq. (25) now yields

$$
D\overline{T}\left(1+\frac{2k^6|A|^2}{\omega^2+k^4}\right)=-K,
\tag{37}
$$

with K obtained from the relation $\int_0^1 D\overline{T}dz=-1$,

$$
K^{-1}=\int_0^1\frac{\omega^2+k^4}{\omega^2+k^4+2k^6|A|^2}dz.
\tag{38}
$$

It follows that $A(z)$ satisfies the nonlinear eigenvalue problem

$$
D^2A-k^2\left(\frac{i\omega}{\sigma}+k^2\right)^2A+\frac{\left(\frac{i\omega}{\sigma}+k^2\right)(k^2-i\omega)}{k^4+\omega^2+2k^6|A|^2}k^2\,\text{Ra}\,KA=0.
\tag{39}
$$

This problem is to be solved for the (complex) eigenfunction $A(z)$ and the eigenvalues Ra K and ω; since K is then determined through (38), an amplitude-Rayleigh number diagram is readily constructed (see below). The corresponding results for steady convection are obtained on setting $\omega=0$.

It is easy to check that traveling rolls (TR) and standing rolls (SR) satisfy an identical eigenvalue problem. Thus in the overstable case there are three patterns with identical time-averaged Nusselt numbers K and frequencies ω in the large Taylor number limit. In fact we know[7,8,13] that in this limit the TR are stable with respect to counter-propagating disturbances while the SR are unstable, an effect that occurs on the slowest of three disparate time scales and hence is absent from the present discussion. Likewise, in the steady case, rolls (R) and squares (S) also satisfy identical eigenvalue problems. This degeneracy between several types of solutions is a consequence of the fact that in the rapid rotation limit the leading nonlinearity is provided by the horizontally averaged temperature profile. As a result, in the weakly nonlinear regime described by (29), the coefficients a and b are equal, and a whole circle of steady solutions $(A_1,A_2)=(1,c)A$, $0\leqslant c\leqslant1$, bifurcates simultaneously. Likewise, in Eqs. (33), $a=b$, $e=2a-2c$ (see below).

Equation (39) is to be solved subject to the boundary conditions,

$$
A(0)=A(1)=0,
\tag{40}
$$

imposing impermeability of the boundaries. These boundary conditions thus correspond to the stress-free case. However,

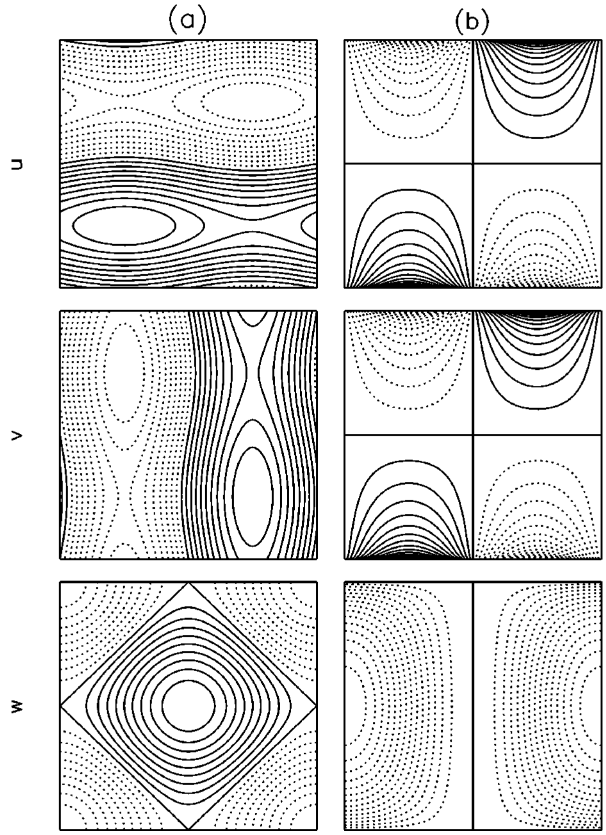

FIG. 2. The velocity field (u,v,w) for a steady solution with a square planform obtained from the nonlinear eigenvalue problem (39) with $\mathrm{Ra}\,E^{4/3}=100(\equiv 11.5\,\mathrm{Ra}_c^{(s)})$ and $k_c^{(s)}E^{1/3}=1.3048$. The Nusselt number $K=83.126$. (a) Horizontal cross section at $z=1/4$ and (b) vertical cross-section at $x=0$. The solutions are plotted using (6) with $E=10^{-3}$. Note that $w(x,y)$ has the symmetry of a *nonrotating* pattern.

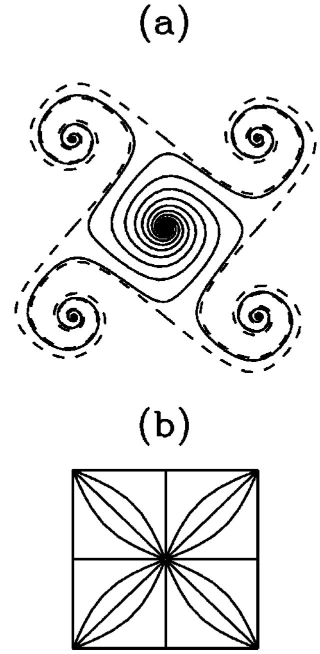

FIG. 3. Streamlines in the plane $z=1/4$ when $\mathrm{Ra}\,E^{4/3}=100$, for comparison with the linear theory streamlines of Refs. 1 and 2 at $\mathrm{Ra}\,E^{4/3}=8.6956$. (a) $E=10^{-3}$ and (b) the nonrotating case $E\to\infty$.

as already discussed, the effect of boundary layers required in the rigid case can be shown to be negligible in the high Taylor number limit. Thus, both sets of boundary conditions give rise to the same nonlinear eigenvalue problem. We solve this problem on a discretized one-dimensional mesh using an iterative Newton–Raphson–Kantorovich (NRK) scheme[18,19] with $\mathcal{O}(10^{-10})$ accuracy in the L_2 norm of $A(z)$ and comparable accuracy in the corresponding eigenvalues K and ω.

In Fig. 2 we show (a) a horizontal cross section at $z=1/4$ and (b) a vertical section taken along the plane $x=0$ of the steady square solution at (scaled) Rayleigh number $\mathrm{Ra}=100$. For comparison, the critical Rayleigh number is $\mathrm{Ra}_c^{(s)}=8.695\,632\,0$. Figure 2 is computed using expression (27) for the horizontal velocity field (u,v) and retaining the nongeostrophic $\mathcal{O}(E^{1/3})$ terms required to satisfy incompressibility and to capture the handedness of the pattern at finite Ekman number ($E=10^{-3}$). Comparable corrections to ϕ arising from higher order corrections in Eqs. (21)–(24) have no effect on the solution symmetry and are omitted. In Fig. 3(a) we show the corresponding streamlines for comparison with the linear eigenfunction streamlines plotted by Veronis[2] and Chandrasekhar.[1] The Z_4 symmetry of the pattern is evident. For contrast, Fig. 3(b) shows the streamlines for a nonrotating square planform ($E\to\infty$). In Fig. 4 we show in an analogous way horizontal and vertical cross-sections for a standing square solution at four equally spaced times within half an oscillation period. Figure 4 also shows the corresponding vertical slices taken parallel to a side. In all cases the cell boundaries are straight. However, as in the SR state,[7] there is no instant in time at which the fluid is wholly at rest. This is illustrated in Fig. 5, where we show the kinetic energy per unit mass, $E\equiv(1/2)\int\mathbf{u}^2dxdydz$, integrated over a cell, as a function of time for several values of Ra. Since $E\equiv\int\mathcal{E}dz$, where

$$\mathcal{E}=\frac{\sigma^2k^2|DA|^2}{\omega^2+\sigma^2k^4}+\frac{k^4}{2}|A|^2 +\left\{\frac{1}{2}\left[\frac{\sigma^2k^2(DA)^2}{(\sigma k^2+i\omega)^2}+\frac{k^4}{2}A^2\right]e^{2i\omega t}+\text{c.c.}\right\}+\mathcal{O}(E^{1/3}), \quad (41)$$

we see that the kinetic energy is strictly positive at all times. Figure 6 shows the time-averaged Nusselt number K, the scaled oscillation frequency ω, and the time-averaged kinetic energy $\overline{E}$ as functions of the Rayleigh number for $\sigma=0.4574$. The corresponding results for steady convection, such as the kinetic energy for a steady square solution,

$$\mathcal{E}=\frac{1}{k^2}|DA|^2+\frac{1}{2}k^4|A|^2+\mathcal{O}(E^{1/3}), \quad (42)$$

are included for comparison. The figures use the preferred wave number in either case, $k=k_c^{(o)}$ and $k_c^{(s)}$, respectively. For the value of the Prandtl number used ($\sigma=0.4574$), oscillatory convection sets in first (Fig. 1) and hence has a larger amplitude than the corresponding steady state with the same wave number at each value of Ra. However, when the preferred wave numbers are used this relationship need not hold, as seen in the Nusselt number plot in Fig. 6(a). Note that K and $\overline{E}$ increase monotonically with Ra, while the os-

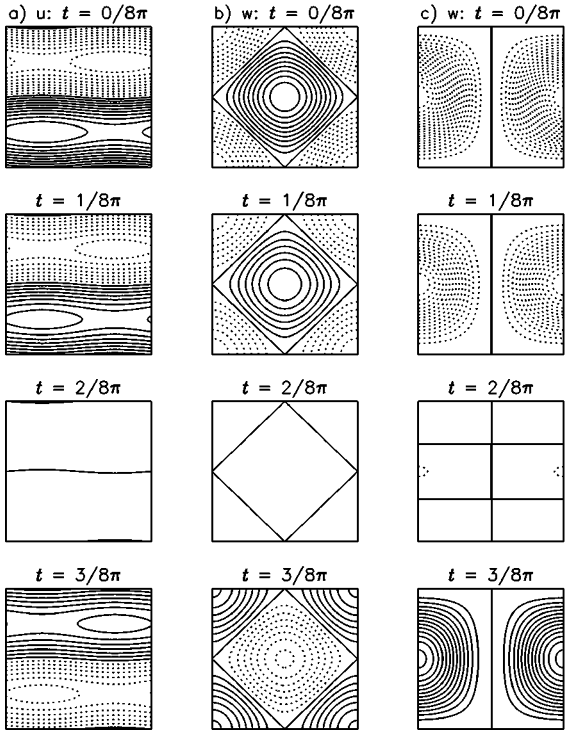

FIG. 4. The velocity field (u,v,w) at $z=1/4$ for a standing square pattern obtained from the nonlinear eigenvalue problem (39) at $\mathrm{Ra}\,E^{4/3}=100$ ($\equiv 18.5\mathrm{Ra}_c^{(o)}$) and $k_c^{(o)}=0.8867$. The Prandtl number $\sigma=0.4574$. The time-averaged Nusselt number $K=93.443$ and the (scaled) oscillation frequency $\omega=0.9547$. The solution is plotted for $E=10^{-3}$ at four equally spaced times during half an oscillation period. The cross sections for v may be obtained by a 90° counterclockwise rotation of u. (c) The corresponding section at $x=0$.

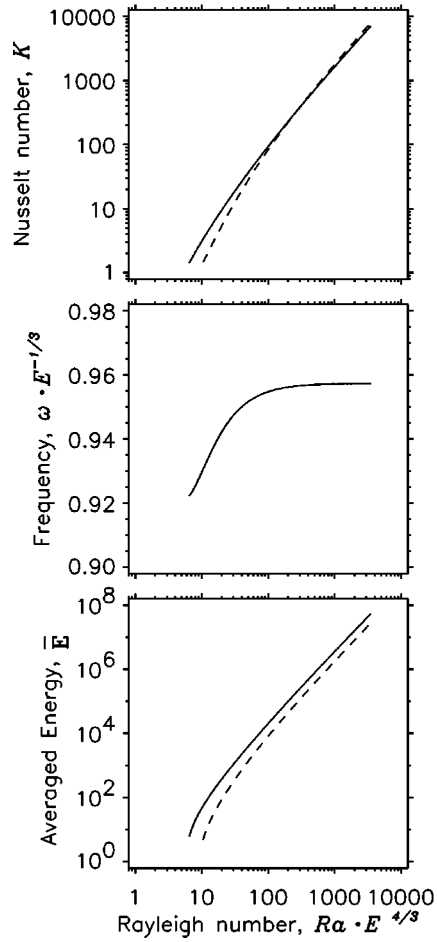

FIG. 6. Time-averaged Nusselt number K, oscillation frequency ω, and time-averaged total kinetic energy $\overline{E}$ as functions of the (scaled) Rayleigh number for square pattern convection when $k_c^{(o)}=0.8867$ and $\sigma=0.4574$. Dashed lines show steady squares, solid lines standing squares.

cillation frequency ω appears to saturate at a finite value. Of course the instantaneous Nusselt number $N(z,t)$ for SR and SS oscillates in time with frequency 2ω and depends on z,[7] while the instantaneous Nusselt number for TR is both time-independent and z-independent (and hence equals K), as required by translation invariance.[20]

In Fig. 7 we show $|A(z)|$ and the corresponding mean temperature profile $\overline{T}(z)$ for both steady and oscillatory convection at several different values of Ra, again for $\sigma=0.4574$. The nonlinear interaction between $\overline{T}$ and the convective motion is responsible for the $\mathcal{O}(1)$ adjustments in $\overline{T}$ which result in the development of thermal boundary layers with increasing Ra. Recent numerical simulations and laboratory experiments on rapidly rotating turbulent convection[6,9] have found, at large Rayleigh numbers, sustained unstable thermal stratification ($D\overline{T}<0$) in the interior of the layer. This profile is set up as a result of boundary layer instabilities leading to plume formation and subsequent lateral mixing due to mutual plume interactions. The organized cellular structure in the present problem necessarily omits this particular aspect and an asymptotically isothermal interior is obtained instead (Fig. 7). We analyze the large Ra solutions to the nonlinear eigenvalue problem in Sec. V.

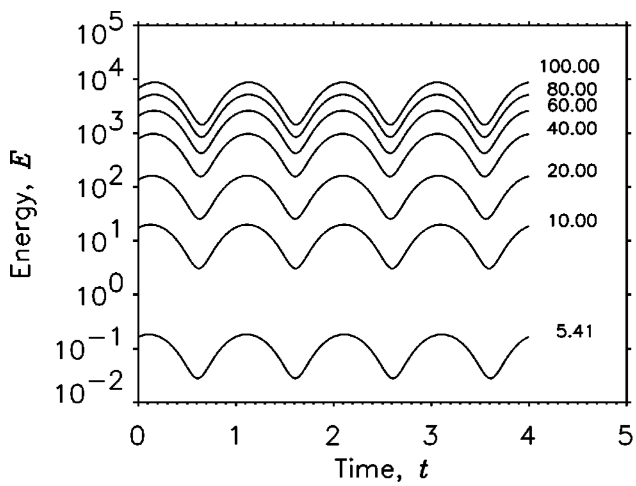

FIG. 5. Total kinetic energy per unit mass $E(t)$ of standing square solutions for $k_c^{(o)}=0.8867$, $\sigma=0.4574$ and several different values of $\mathrm{Ra}\,E^{4/3}$.

It remains to comment on the dependence of these results on the wave number k. The linear theory[1,7] shows that oscillatory onset occurs for $k<k_{\mathrm{TB}}\approx 1.2422$. At the Takens–Bogdanov point, $k=k_{\mathrm{TB}}$, the oscillation frequency vanishes. Although this point is shielded by oscillatory onset at different wave numbers, as indicated in Fig. 1(a), the linear theory suggests that oscillations cannot be present for $k>k_{\mathrm{TB}}$. In fact we find that this is not so. Figure 8 shows that nonlinear

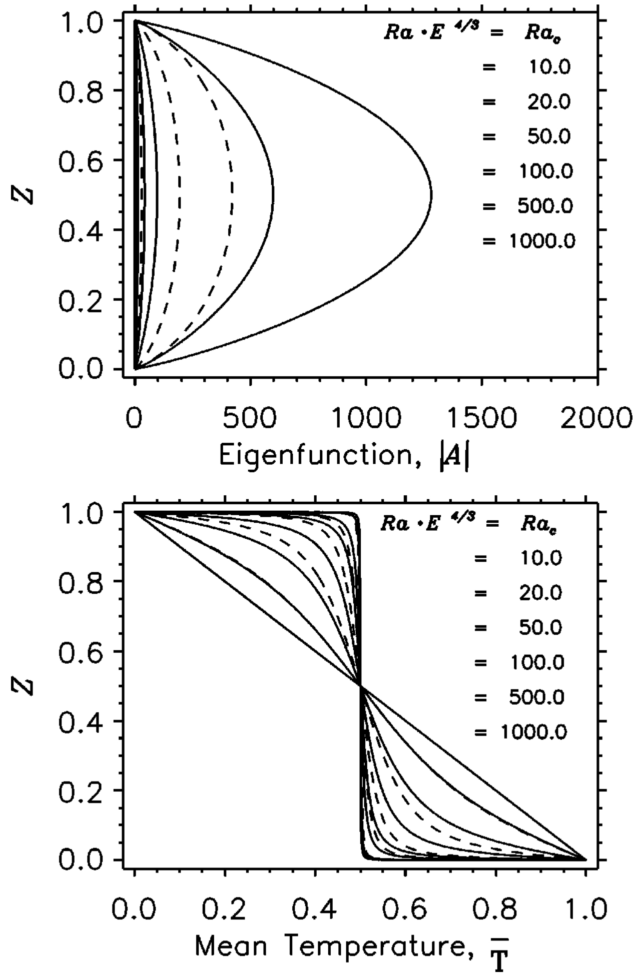

FIG. 7. (a) $|A(z)|$ and (b) $\overline{T}(z)$ for steady (dashed lines) and standing (solid lines) squares, at several different values of the (scaled) Rayleigh number, $k_c^{(s)}=1.3048$ and $k_c^{(o)}=0.8867$, respectively. The Prandtl number $\sigma=0.4574$.

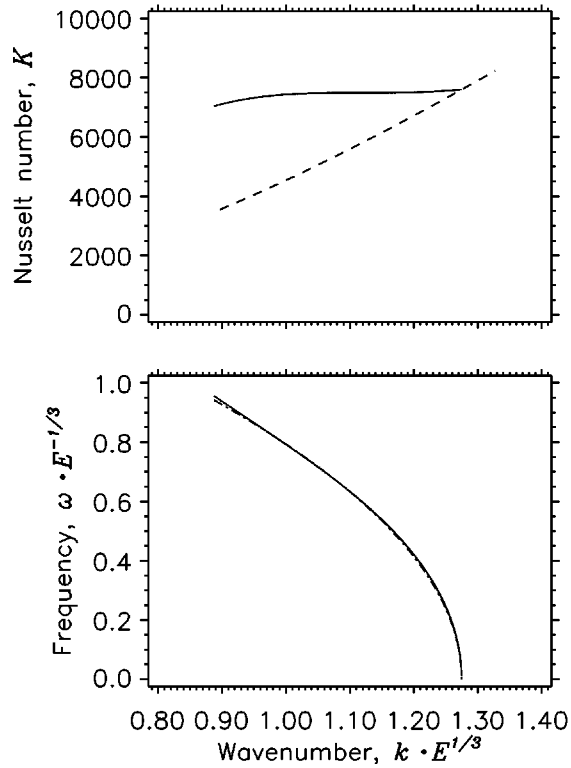

FIG. 8. (a) The time-averaged Nusselt number K for oscillatory (solid line) and steady (dashed line) convection and (b) oscillation frequency ω, as functions of k for $\sigma=0.4574$, and Ra$=3500$. The oscillatory branch terminates in a steady-state bifurcation at $k=k_c\approx 1.274\,727\,0$ with $\omega\approx 1.513\,770\,4(k_c-k)^{1/2}$ near k_c [dashed-dotted curve plot in (b)].

oscillations can be found by starting with $k<k_{\mathrm{TB}}$, increasing the Rayleigh number to a high value, and then increasing k at constant Ra. The figure shows that in this case the oscillations terminate on the branch of steady states at finite amplitude and do so in a secondary Takens–Bogdanov bifurcation, i.e., the oscillation frequency ω vanishes as the square root of the distance from the termination point [see Fig. 8(b)]. Thus in our system the transfer of stability from oscillatory to steady convection occurs via a steady-state bifurcation of the type usually associated with a parity-breaking bifurcation from a circle of steady states to traveling rolls. This is so despite the fact that we can use our solutions to construct both standing and traveling wave states. However, our SR solutions necessarily have a zero mean [see Eq. (35)] and hence cannot undergo the gluing bifurcation that would allow them to terminate on the roll branch in a secondary Hopf bifurcation. Thus for the SR, the Takens–Bogdanov bifurcation represents the coalescence of a gluing bifurcation with a secondary Hopf bifurcation.

C. Alternating rolls and traveling squares

The alternating rolls (AR) and traveling squares (TS) have a more complicated horizontal structure and cannot be found by the above methods at finite amplitude. This is because the various horizontal Jacobians do not vanish for these solutions. However, the existence of these solutions has important implications for the stability of the TR, SR, and SS states already found. In this section we compute these two states at small amplitude and examine their implications for the finite amplitude states already found.

Specifically, we write

$$\psi=\epsilon\psi_0+\epsilon^2\psi_1+\epsilon^3\psi_2+\cdots,$$
$$\mathrm{Ra}=\mathrm{Ra}_c^{(o)}(1+\epsilon^2\mu+\cdots),\quad \omega=\omega_c^{(o)}+\epsilon^2\omega_2+\cdots, \tag{43}$$

with similar expressions for the fields ϕ, θ, and $\overline{T}$. We also need to expand the constant K in (38). From Eqs. (21)–(24) we now find

$$\psi_0=\tfrac{1}{2}e^{i\omega t}\{A_1e^{ikx}+A_2e^{iky}+A_3e^{-ikx}+A_4e^{-iky}\}\sin\pi z+\mathrm{c.c.},$$
$$\phi_0=\tfrac{1}{2}e^{i\omega t}\{B_1e^{ikx}+B_2e^{iky}+B_3e^{-ikx}+B_4e^{-iky}\}\cos\pi z+\mathrm{c.c.},$$
$$\theta_0=\tfrac{1}{2}e^{i\omega t}\{C_1e^{ikx}+C_2e^{iky}+C_3e^{-ikx}+C_4e^{-iky}\}\sin\pi z+\mathrm{c.c.}, \tag{44}$$

where

$$B_j=\frac{\pi}{\frac{i\omega}{\sigma}+k^2}A_j,\quad C_j=\frac{k^2}{i\omega+k^2}A_j,\quad j=1,...,4. \tag{45}$$

At $\mathcal{O}(\epsilon^2)$, we need to compute the horizontal Jacobians and solve the resulting equations for ψ_1, ϕ_1, and θ_1. We find that

$$\psi_1=\frac{1}{8}\{A_5e^{ikx+iky}+A_6e^{ikx-iky}+\text{c.c.}\}\sin 2\pi z,$$

$$\phi_1=\frac{\pi}{4}\{B_5e^{ikx+iky}+B_6e^{ikx-iky}+\text{c.c.}\}\cos 2\pi z, \tag{46}$$

$$\theta_1=\frac{1}{8}\{C_5e^{ikx+iky}+C_6e^{ikx-iky}+\text{c.c.}\}\sin 2\pi z,$$

with $A_5\dots C_6$ determined in terms of $A_1\dots A_4$. At $\mathcal{O}(\epsilon^3)$ we obtain four nontrivial solvability conditions by eliminating the four types of resonant terms appearing in the linear solution. These equations have the form (33) predicted abstractly with the following coefficients:

$$a=b=-\frac{1}{8\Delta_0}\frac{k^6}{\omega^2+k^4}, \tag{47}$$

$$c=d=-\frac{1}{8\Delta_0}\frac{k^6}{\omega^2+k^4}+\frac{\pi}{16\Delta_0}\left(\frac{\Delta}{i\omega+k^2}+\frac{\Delta'}{\frac{i\omega}{\sigma}+k^2}\right)+\frac{\pi\Delta(i\omega+k^2)}{16\sigma\,\text{Ra}\,\Delta_0}\left(1+\frac{2k^2}{\frac{i\omega}{\sigma}+k^2}-\frac{\pi^2}{k^2\left(\frac{i\omega}{\sigma}+k^2\right)^2}\right), \tag{48}$$

where

$$\Delta_0=\frac{2\omega}{\sigma}\left[\frac{\omega k^2(1+\sigma)+i(\omega^2+\sigma(1+2\sigma)k^4)}{\omega^2+\sigma^2k^4}\right], \tag{49}$$

$$\Delta=\frac{2i\omega\pi k^4}{\omega^2+\sigma^2k^4}\frac{\left[1+\frac{\sigma(1-\sigma)\text{Ra}}{2(\omega^2+k^4)}\right]}{\text{Ra}-\frac{2\pi^2}{k^2}-4k^4}, \tag{50}$$

$$\Delta'=\frac{2i\omega\pi k^4}{\omega^2+\sigma^2k^4}\frac{\left[1+\left(\frac{\pi^2}{k^2}+2k^4\right)\frac{\sigma(1-\sigma)}{\omega^2+k^4}\right]}{\text{Ra}-\frac{2\pi^2}{k^2}-4k^4}, \tag{51}$$

and

$$e=2a-2c. \tag{52}$$

In these expressions ω, k, and Ra denote their critical values $\omega_c^{(o)}$, $k_c^{(o)}$, and $\text{Ra}_c^{(o)}$, respectively. Note that all the coefficients are complex, although they are not all independent. In particular, $c=d$ as predicted on the basis of the extra reflection symmetry (26). We expect, therefore, solutions in the form of TR, SR, SS, AR, and TS guaranteed by the abstract theory. Specifically, for SS($A_1=A_2=A_3=A_4\equiv A$), we find

$$\nu A+4a|A|^2A=0, \tag{53}$$

as obtained from the small amplitude limit of the nonlinear eigenvalue problem (39). Similar expressions hold for TR and SR. For AR($A_1=A_3=-iA_2=-iA_4\equiv A$) we obtain

$$\nu A+4c|A|^2A=0, \tag{54}$$

while the TS ($A_1=A_2=A$, $A_3=A_4=0$) are given by

$$\nu A+(a+c)|A|^2A=0. \tag{55}$$

Since $a_r<0$, $c_r<0$ for all values of σ for which oscillations are present, all solutions bifurcate supercritically. Finally, the relations (47) and (52) among the coefficients prevent the existence of an unstable pattern called standing cross-rolls (SCR).

As shown by Silber and Knobloch,[14] the stability of the five competing solutions (SR, TR, SS, AR, and TS) depends on the nonlinear coefficients $a,\dots,e$. Because of the degenerate nature of these equations in the present problem we find that the stability properties of the first three patterns are identical and involve zero eigenvalues that are not forced by translation invariance. It is these eigenvalues that become nonzero if higher order terms in the asymptotic expansion are retained and describe the competition among these patterns on a slower time scale. The abstract theory, applied to the present problem, also shows that SS and AR cannot be stable simultaneously. In fact, it is possible to show analytically that $c_r<a_r<0$ and hence that the AR are always unstable. Moreover, the relations (47) and (52) imply that TS are also always unstable. In fact, the $\mathcal{O}(E^{1/3})$ terms omitted from the asymptotic Eqs. (21)–(24) turn the TS into a secondary branch,[12] but this branch will inherit the unstable eigenvalue present in the rapid rotation limit and so will be unstable. Thus only TR, SR, and SS are candidates for a stable pattern, and these are precisely the patterns accessible to the fully nonlinear theory.

V. OTHER PLANFORMS

In this section we extend the previous analysis to other planforms of interest. To this end we introduce the planform function $h(x,y)$ satisfying the planform equation

$$\nabla_\perp^2 h+k^2h=0. \tag{56}$$

The planforms of interest are solutions to this Helmholtz equation that are periodic in the plane. The square planform encountered in Sec. IV is an example of such a planform. Other planforms include rolls ($h=\cos kx$), hexagons $[h(x,y)=\cos kx+\cos(\frac{1}{2}kx+(\sqrt{3}/2)ky)+\cos(\frac{1}{2}kx-(\sqrt{3}/2)ky)]$, regular triangles $[h(x,y)=\sin kx+\sin(\frac{1}{2}kx+(\sqrt{3}/2)ky)+\sin(\frac{1}{2}kx-(\sqrt{3}/2)ky)]$, patchwork quilt $[h(x,y)=\cos(\frac{1}{2}kx+(\sqrt{3}/2)ky)+\cos(\frac{1}{2}kx-(\sqrt{3}/2)ky)]$, all of which represent solutions on the hexagonal lattice.[21] We use the terminology patchwork quilt to distinguish this special solution from general rectangles which also satisfy the planform equation $[h(x,y)=\cos mx+\cos ny,\ m^2+n^2=k^2]$. As in the case of the square lattice patterns, the reflection symmetry (26) continues to exert an important influence.

A. Steady convection

Suppose first that a pair of rolls with wave vectors $\mathbf{k}_1=(k,0)$ and $\mathbf{k}_2=(k\cos\alpha,k\sin\alpha)$ are unstable. Then, because of the reflection (26), rolls with wave vector $\mathbf{k}_3=(k\cos\alpha,-k\sin\alpha)$ are also unstable. Consequently, one cannot restrict attention to rolls with the two wave vectors $\mathbf{k}_1,\mathbf{k}_2$ unless $\alpha=\pi/2$. This is the square lattice considered above; the rhombic lattice appropriate to bifurcations in generic rotating systems[15] cannot arise in the present problem. Consequently, there are no Küppers–Lortz-like instabilities at leading order in the rapid rotation limit.

The remaining possibility is that the vector $\mathbf{k}_3$ is independent of the other two. In that case spatially periodic patterns are obtained only if $\mathbf{k}_2+\mathbf{k}_3=\mathbf{k}_1$, i.e., $\alpha=\pi/3$. The problem is then posed on the hexagonal lattice, and once again the symmetry (26) implies the more restrictive symmetry group $D_6\times T^2$ instead of the expected[22] symmetry $Z_6\times T^2$. The steady-state bifurcation with this symmetry (together with the midplane reflection symmetry) was analyzed by Golubitsky *et al.*,[21] who identified the presence of four primary solution branches, rolls (R), hexagons (H), regular triangles (RT), and the patchwork quilt (PQ), as discussed above. All of these solutions are equally efficient at transporting heat, as we now show.

We suppose that

$$(\psi,\phi,\theta)=(A(z),B(z),C(z))h(x,y), \tag{57}$$

where h satisfies the planform Eq. (56). It follows that Eqs. (36) are unchanged while

$$D\overline{T}(1+k^2\overline{h^2}|A|^2)=-K, \tag{58}$$

where

$$K^{-1}=\int_0^1\frac{dz}{1+k^2\overline{h^2}|A|^2}. \tag{59}$$

The eigenfunction $A(z)$ thus solves the nonlinear eigenvalue problem,

$$D^2A-k^2\left(k^4-\frac{\mathrm{Ra}\,K}{1+k^2\overline{h^2}|A|^2}\right)A=0, \tag{60}$$

for the eigenvalue Ra K. Since the quantity $\overline{h^2}$ can be absorbed in the amplitude it follows that all planforms with the same value of k have the same Nusselt number K. Note that the eigenvalue problem depends on $|A|^2$ only, even if the boundary conditions on Eqs. (1)–(3) differ at top and bottom. This is because in the rapid rotation limit the effective boundary conditions are simply (40). In this limit the problem therefore acquires an additional reflection symmetry and there is no distinction between $\pm$ hexagons, both of which bifurcate supercritically. Horizontal cross-sections of the resulting three-dimensional states are shown in Fig. 9 for $E=10^{-3}$. The corresponding streamlines are shown in Fig. 10 along with their nonrotating counterparts ($E\to\infty$) for comparison.

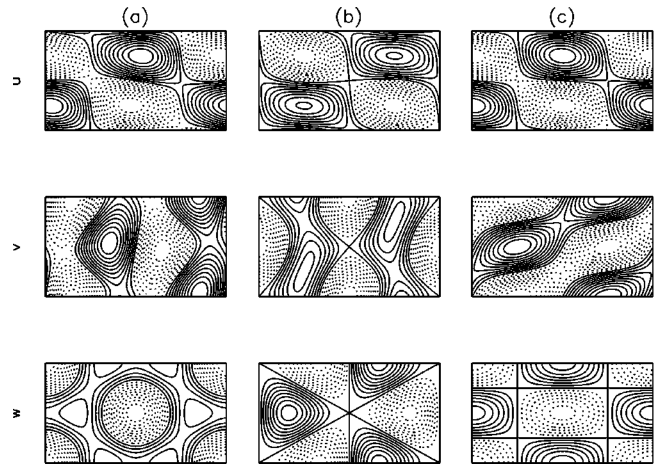

FIG. 9. The velocity field (u,v,w) at $z=1/4$ steady for (a) down-hexagons, (b) regular triangles, and (c) patchwork quilt at Ra $E^{4/3}=100$, $\sigma=0.4574$. The figures are drawn for $E=10^{-3}$. Solid (dotted) contours indicate positive (negative) values. Note that $w(x,y)$ has the symmetry of a *nonrotating* pattern.

B. Overstable convection

For overstable convection on the hexagonal lattice, the symmetry (26) also implies that the spatial symmetry group of the problem is $D_6\times T^2$ instead of the expected symmetry $Z_6\times T^2$. The generic Hopf bifurcation with this symmetry was analyzed by Roberts *et al.*[23] These authors identified 11 primary solution branches, all of which bifurcate simultaneously, and we must therefore expect corresponding solutions to Eqs. (21)–(24).

As in the square planform case not all of these states can be obtained in the fully nonlinear regime. For those that can, we write

$$\begin{aligned}(\psi,\phi,\theta)=&\tfrac{1}{2}(A(z)e^{i\omega t}h+A^*(z)e^{-i\omega t}h^*,\\ &B(z)e^{i\omega t}h+B^*(z)e^{-i\omega t}h^*,C(z)e^{i\omega t}h+C^*(z)e^{-i\omega t}h^*),\end{aligned} \tag{61}$$

where $h(x,y)$ once again satisfies the planform Eq. (56). However, this time not all such h are allowed, cf. Sec. IV C. To determine the admissible h we compute the Jacobian $J(\phi,\theta)$,

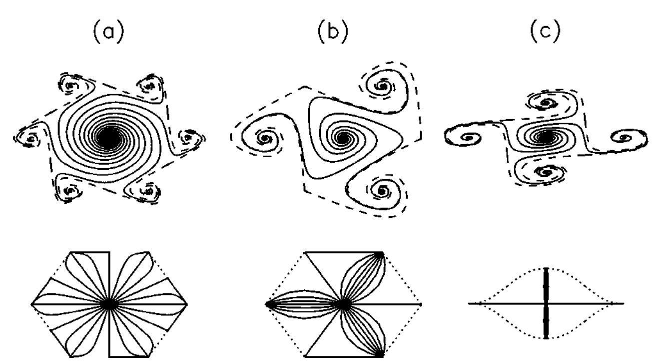

FIG. 10. Streamlines at $z=1/4$ for steady rotating ($E=10^{-3}$: upper panels) and nonrotating ($E\to\infty$: lower panels) (a) down-hexagons, (b) regular triangles, and (c) patchwork quilt when Ra $E^{4/3}=100$, $\sigma=0.4574$ for comparison with the linear theory streamlines of Refs. 1 and 2.

TABLE I. The 11 nontrivial solutions of Eqs. (66) identified and illustrated by Roberts *et al.* (Ref. 23). The bracketed patterns have identical properties within the truncated normal form (66).

Standing rolls (SR)	:	$(r,0,0,r,0,0)$
Standing hexagons (SH)	:	(r,r,r,r,r,r) }
Standing regular triangles (SRT)	:	$(r,r,r,-r,-r,-r)$ }
Standing patchwork quilt (SPQ)	:	$(0,r,r,0,r,r)$
Oscillating triangles (OT)	:	$(r,r,r,0,0,0)$
Wavy rolls 1 (WR1)	:	$(r,0,r,r,0,-r)$
Twisted patchwork quilt (TwPQ)	:	$(r,re^{2\pi i/3},re^{4\pi i/3},r,re^{2\pi i/3},re^{4\pi i/3})$ }
Wavy rolls 2 (WR2)	:	$(r,re^{2\pi i/3},re^{4\pi i/3},-r,-re^{2\pi i/3},-re^{4\pi i/3})$ }
Traveling rolls (TR)	:	$(r,0,0,0,0,0)$
Traveling patchwork quilt 1 (TPQ1)	:	$(r,0,r,0,0,0)$
Traveling patchwork quilt 2 (TPQ2)	:	$(r,0,0,0,0,r)$

$$J(\phi,\theta)=\tfrac{1}{4}(BC^*-B^*C)(\partial_x h\partial_y h^*-\partial_x h^*\partial_y h). \tag{62}$$

It follows that the admissible h must satisfy $\partial_x h\partial_y h^*-\partial_x h^*\partial_y h=0$ in addition to (56). If this is so the procedure of Sec. IV yields the eigenvalue problem

$$D^2A-k^2\left(\frac{i\omega}{\sigma}+k^2\right)^2A+\frac{\left(\frac{i\omega}{\sigma}+k^2\right)(k^2-i\omega)}{k^4+\omega^2+\frac{k^6}{2}\overline{h^2|A|^2}}k^2\,\mathrm{Ra}\,K\,A$$
$$=0, \tag{63}$$

where

$$K^{-1}=\int_0^1\frac{\omega^2+k^4}{\omega^2+k^4+\frac{1}{2}k^6\overline{h^2|A|^2}}dz. \tag{64}$$

To identify the states for which the preceding analysis applies we write

$$(\psi,\phi,\theta)=\tfrac{1}{2}(A(z),B(z),C(z))e^{i\omega t}\{A_1e^{i\mathbf{k}_1\cdot\mathbf{x}}+As2\}$$
$$\times e^{i\mathbf{k}_2\cdot\mathbf{x}}+A_3e^{i\mathbf{k}_3\cdot\mathbf{x}}+A_4e^{-i\mathbf{k}_1\cdot\mathbf{x}}+A_5e^{-i\mathbf{k}_2\cdot\mathbf{x}}$$
$$+A_6e^{-i\mathbf{k}_3\cdot\mathbf{x}}\}+\mathrm{c.c.}+\mathcal{O}(E^{1/3}), \tag{65}$$

where $\mathbf{k}_1=k_c^{(0)}\hat{\mathbf{x}}$, $\mathbf{k}_{2,3}=(k_c^{(0)}/2)(-\hat{\mathbf{x}}\pm\sqrt{3}\hat{\mathbf{y}})$. An examination of this planform function readily shows that $\partial_x h\partial_y h^*-\partial_x h^*\partial_y h=0$ for the planforms called TR, SR, SH, SRT, and SPQ (see Table I). All of these states have the same time-averaged Nusselt numbers K and the same nonlinear frequency ω, and bear the same relationship to their steady counterparts as the standing squares.

The abstract analysis of the Hopf bifurcation with $D_6\times T^2$ symmetry by Roberts *et al.*[23] finds six other solutions at small amplitude. While these do not satisfy the condition $\partial_x h\partial_y h^*-\partial_x h^*\partial_y h=0$, and hence cannot be found at finite amplitude by the methods of this paper, they can be found at small amplitude by reducing Eqs. (21)–(24) to the appropriate normal form. Truncated at third order these equations are

$$\dot{A}_1=\mu(\lambda)A_1+a|A_1|^2A_1+b|A_4|^2A_1$$
$$+c(|A_2|^2+|A_3|^2)A_1+d(|A_5|^2+|A_6|^2)A_1$$
$$+e(A_2A_5+A_3A_6)\bar{A}_4. \tag{66}$$

Here a, b, c, d, and e are complex coefficients. The corresponding equations for $A_2,\ldots,$ are obtained by a cyclic interchange of 1, 2, and 3 and the symmetry $\mathbf{x}\to-\mathbf{x}$.

As in the case of the square lattice, these equations can be reduced to a set of six algebraic equations by requiring that $\mathring{\mathbf{A}}=i(\omega-\omega_c^{(o)})\mathbf{A}$. We proceed as in Sec. IV C. Omitting all details, we find that at $\mathcal{O}(\epsilon^3)$ equations of the form (66) with

$$a=b=-\frac{1}{8\Delta_0}\frac{k^6}{\omega^2+k^4}, \tag{67}$$

$$c=-\frac{1}{8\Delta_0}\frac{k^6}{\omega^2+k^4}+\frac{\pi\sqrt{3}}{96\Delta_0}\left(\frac{2\Delta_2}{i\omega+k^2}+\frac{3\Delta_2'}{\frac{i\omega}{\sigma}+k^2}\right)$$
$$+\frac{\pi\sqrt{3}\Delta_2(i\omega+k^2)}{96\sigma\,\mathrm{Ra}\,\Delta_0}\left(2+\frac{9k^2}{\frac{i\omega}{\sigma}+k^2}-\frac{4\pi^2}{k^2\left(\frac{i\omega}{\sigma}+k^2\right)^2}\right), \tag{68}$$

$$d=-\frac{1}{8\Delta_0}\frac{k^6}{\omega^2+k^4}+\frac{\pi\sqrt{3}}{32\Delta_0}\left(\frac{2\Delta_1}{i\omega+k^2}+\frac{\Delta_1'}{\frac{i\omega}{\sigma}+k^2}\right)$$
$$+\frac{\pi\sqrt{3}\Delta_1(i\omega+k^2)}{32\sigma\,\mathrm{Ra}\,\Delta_0}\left(2+\frac{k^2}{\frac{i\omega}{\sigma}+k^2}\right), \tag{69}$$

and

$$e=2a-c-d. \tag{70}$$

Here

$$\Delta_0=\frac{2\omega}{\sigma}\left[\frac{\omega k^2(1+\sigma)+i(\omega^2+\sigma(1+2\sigma)k^4)}{\omega^2+\sigma^2k^4}\right], \tag{71}$$

$$\Delta_1=\frac{i\omega\pi\sqrt{3}k^4}{\omega^2+\sigma^2k^4}\frac{\left[1+\frac{\sigma(1-\sigma)\mathrm{Ra}}{\omega^2+k^4}\right]}{\mathrm{Ra}-\frac{4\pi^2}{k^2}-k^4}, \tag{72}$$

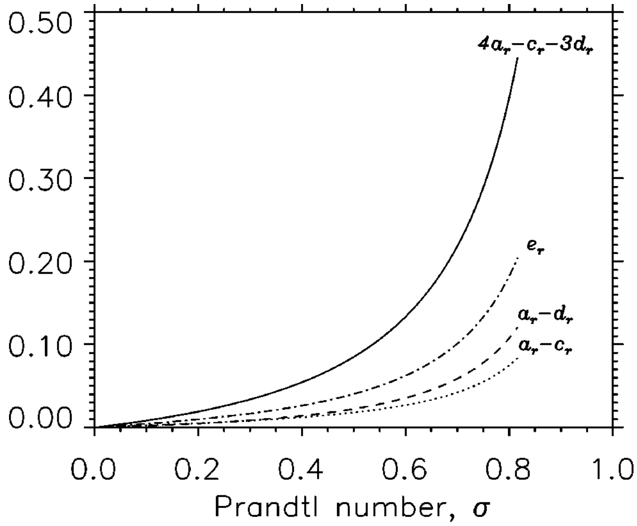

FIG. 11. The quantities $a_r - c_r$, $a_r - d_r$, e_r, and $4a_r - c_r - 3d_r$ from Eqs. (67) and (70) at onset ($k = k_c^{(o)}$, $\omega = \omega_c^{(o)}$, $\mathrm{Ra} = \mathrm{Ra}_c^{(o)}$) as a function of the Prandtl number σ.

$$\Delta_2 = \frac{i\omega\pi\sqrt{3}k^4}{\omega^2+\sigma^2k^4}\,\frac{\left[1+\dfrac{\sigma(1-\sigma)\mathrm{Ra}}{3(\omega^2+k^4)}\right]}{\mathrm{Ra}-\dfrac{4\pi^2}{3k^2}-9k^4}, \tag{73}$$

$$\Delta_1' = \frac{i\omega\pi\sqrt{3}k^4}{\omega^2+\sigma^2k^4}\,\frac{\left[1+\dfrac{\sigma(1-\sigma)}{\omega^2+k^4}\left(k^4+\dfrac{4\pi^2}{k^2}\right)\right]}{\mathrm{Ra}-\dfrac{4\pi^2}{k^2}-k^4}, \tag{74}$$

and

$$\Delta_2' = \frac{i\omega\pi\sqrt{3}k^4}{\omega^2+\sigma^2k^4}\,\frac{\left[1+\dfrac{\sigma(1-\sigma)}{3(\omega^2+k^4)}\left(9k^4+\dfrac{4\pi^2}{3k^2}\right)\right]}{\mathrm{Ra}-\dfrac{4\pi^2}{3k^2}-9k^4}. \tag{75}$$

In these expressions ω, k, and Ra denote their critical values $\omega_c^{(o)}$, $k_c^{(o)}$, $\mathrm{Ra}_c^{(o)}$, respectively.

Once again, the five solutions TR, SR, SH, SRT, and SPQ all bifurcate supercritically because $\alpha_r < 0$. The stability properties of the remaining solutions can be determined using the results obtained by Roberts *et al.*[23] As in the square case, each solution has a zero eigenvalue that is not forced by symmetry but that vanishes in the rapid rotation limit. Since $a_r - c_r > 0$, $a_r - d_r > 0$, $e_r > 0$, $4a_r - c_r - 3d_r > 0$ for all values of the Prandtl number σ (see Fig. 11), these five solutions are all candidates for a stable pattern, in the sense that modulo the zero eigenvalue all are stable near onset. In contrast the remaining solutions, OT, WR1, TwPQ, WR2, TPQ1, and TPQ2 are all unstable. As on the square lattice, the candidates for stable patterns are precisely those patterns for which the fully nonlinear theory works, i.e., those patterns for which $\partial_x h \partial_y h^* - \partial_x h^* \partial_y h = 0$. In fact we know, from general theory, that SH and SRT cannot be stable simultaneously. This is a consequence of omitted fifth-order terms in the expansion (66). However, an expansion of the nonlinear eigenvalue problem shows that in the present case these terms are absent, i.e., the selection between SH and SRT occurs as a result of $\mathcal{O}(E^{1/3})$ corrections only. These corrections are also responsible for shifting the unforced zero eigenvalue away from the origin and hence for any weak instabilities of the remaining candidates.

VI. HIGHLY SUPERCRITICAL CONVECTION

It is of considerable theoretical interest to look at the behavior of the (time-averaged) Nusselt number at highly supercritical Rayleigh numbers. For the case of steady convection such an analysis was carried out already by Bassom and Zhang.[4] The overstable case is very similar because the oscillation frequency saturates with increasing Rayleigh number (see Fig. 7). The complex eigenvalue problem (38) and (39) can be written in the form

$$D^2\rho - \rho(D\vartheta)^2 - k^2\left(k^4 - \frac{\omega^2}{\sigma^2}\right)\rho + \frac{\mathrm{Ra}\,Kk^2\left(\dfrac{\omega^2}{\sigma}+k^4\right)}{\omega^2+k^4+2k^6\rho^2}\,\rho = 0, \tag{76}$$

$$D(\rho^2 D\vartheta) - \frac{2\omega}{\sigma}k^4\rho^2 + \frac{\mathrm{Ra}\,Kk^4\omega(1-\sigma)}{\sigma(\omega^2+k^4+2k^6\rho^2)}\,\rho^2 = 0, \tag{77}$$

where $A \equiv \rho e^{i\vartheta}$. In the large Ra limit we expect ρ and K to be large, but $\omega = \mathcal{O}(1)$. We define

$$\rho = \rho_0 f(z), \quad \mathrm{Ra}\,K = \lambda_\infty \rho_0^2, \quad \omega = \omega_\infty, \tag{78}$$

where ρ_0 measures the maximum value of $|A(z)|$, i.e., $|f(z)| \leq 1$, and is assumed to be large. Since k remains fixed, the eigenvalue problem becomes

$$D^2 f - f(D\vartheta)^2 - k^2\left(k^4 - \frac{\omega_\infty^2}{\sigma^2}\right)f + \frac{\lambda_\infty}{2k^4 f}\left(\frac{\omega_\infty^2}{\sigma}+k^4\right) = 0, \tag{79}$$

$$D(f^2 D\vartheta) - \frac{2\pi_\infty}{\sigma}k^4 f^2 + \frac{\lambda_\infty\omega_\infty(1-\sigma)}{2\sigma k^2} = 0, \tag{80}$$

at leading order in ρ_0^{-1}. These two equations, subject to the boundary conditions $f(0) = Df(1/2) = 0$, $f(1/2) = 1$, $D\vartheta(1/2) = 0$, constitute an eigenvalue problem for λ_∞ and ω_∞. With the above scaling the contribution from the bulk to K^{-1} is $\mathcal{O}(\rho_0^{-2})$ and hence smaller than that from the thermal boundary layers. In the boundary layers the term $f(D\vartheta)^2$ in Eq. (79) is subdominant, as will be verified *a posteriori*, so that (79) can be integrated once,

$$\frac{1}{2}(Df)^2 = -\frac{1}{2}k^2\left(k^4 - \frac{\omega_\infty^2}{\sigma^2}\right)(1-f^2) - \frac{\lambda_\infty}{2k^4}\left(\frac{\omega_\infty^2}{\sigma}+k^4\right)\ln f. \tag{81}$$

Thus at leading order,

$$f = \hat{f}z(-\ln z)^{1/2}, \quad \hat{f} = \frac{\sqrt{\lambda_\infty}}{k^2}\left(\frac{\omega_\infty^2}{\sigma}+k^4\right)^{1/2}. \tag{82}$$

In the following we therefore introduce the boundary layer coordinate

$$Z=\rho_0(\ln\rho_0)^{1/2}z, \quad Z=\mathcal{O}(1). \tag{83}$$

It follows therefore that to leading order

$$K=K_0\rho_0(\ln\rho_0)^{1/2}, \quad K_0=\frac{k}{\pi}\sqrt{\frac{2\lambda_\infty}{\sigma}}\left(\frac{\omega_\infty^2+\sigma k^4}{\omega_\infty^2+k^4}\right)^{1/2}, \tag{84}$$

so that

$$\mathrm{Ra}=\frac{\lambda_\infty}{K_0}\rho_0(\ln\rho_0)^{-1/2}. \tag{85}$$

These relations imply a transcendental relation between the Nusselt and Rayleigh numbers when the latter is large,

$$K=K_1\,\mathrm{Ra}\ln(K\,\mathrm{Ra}), \quad K_1=\frac{k^2}{\pi^2\sigma}\left(\frac{\omega_\infty^2+\sigma k^4}{\omega_\infty^2+k^4}\right), \tag{86}$$

to leading order.

It remains to verify that in the boundary layer one can indeed neglect the term $f(D\vartheta)^2$ in Eq. (79) and to determine the eigenvalues λ_∞ and ω_∞. To this end we take the boundary layer solution (82) and solve Eq. (23). To leading order we find that $f(D\vartheta)^2\approx z^{-1}(-\ln z)^{-3/2}$, and hence that this term is small compared with the f^{-1} term retained in obtaining Eq. (82). The eigenvalues λ_∞ and ω_∞ are most easily found by extrapolation of the solutions of the eigenvalue problem (39). The latter quantity determines the constant K_1 in the asymptotic relation (86) and allows us to compare the asymptotic prediction (86) with solutions of the nonlinear eigenvalue problem (39). This comparison is shown in Fig. 12(a), together with the approach of the eigenvalue $\lambda \equiv \mathrm{Ra}\,K/\rho_0^2$ to its asymptotic value λ_∞ [Fig. 12(b)] and the Prandtl number dependence of K_1 [Fig. 12(c)].

The above analysis applies straightforwardly to the real eigenvalue problem describing steady convection. It suffices to drop the ϑ variable and set $\omega_\infty=0$. Consequently, a relation of the form (86) governs the steady problem as well,[4] with the constant K_1 replaced by $K_1=k^2/\pi^2$. Once again this relation is independent of the eigenvalue λ.

It will be recalled that upper bound theory[24] for nonrotating convection shows that for large Rayleigh numbers the Nusselt number $K(\mathrm{Ra})<(3\,\mathrm{Ra}/64)^{1/2}$; a single mode version of this theory gives a more restrictive upper bound: $K(\mathrm{Ra})<(\mathrm{Ra}/248)^{3/8}$. Since rotation drops out from the power integrals used in the derivation of these results, these upper bounds hold for rotating convection as well. However, these results do not contradict the asymptotic behavior obtained from the nonlinear eigenvalue problem. The upper bound results are obtained for finite rotation in the limit $\mathrm{Ra}\to\infty$. In contrast, in the derivation of the eigenvalue problem we first let $\mathrm{Ta}\to\infty$ and then examine the Nusselt number at large values of Ra. Evidently the two limiting procedures, $\mathrm{Ra}\to\infty$ and $\mathrm{Ta}\to\infty$, do not commute.

VII. DISCUSSION AND CONCLUSION

In this paper, we have derived by an asymptotic expansion in the Ekman number a reduced set of dynamical equations describing rapidly rotating convection. These equations, summarized in (21)–(24), promise to have significant applications, for example, to the study of rapidly rotating turbulent convection.[5] The scaling adopted in deriving these equations implies that all three components of the velocity field are $\mathcal{O}(E^{-1/3})$ and hence large. It is this property that makes the resulting equations valid for any $\mathcal{O}(E^{-4/3})$ value of the Rayleigh number. As a result, the reduced equations are valid well beyond the regime in which weakly nonlinear theory applies and thus describe strongly nonlinear three-dimensional convection. In particular, the equations describe correctly the nonlinear deformation of the temperature profile with increasing supercriticality. It should be noted that in studies of two-dimensional rapidly rotating convection,[4,7] the adopted scaling is anisotropic, although the same nonlinear eigenvalue problem is recovered at the end. The reason for this can be seen from expression (6) for the velocity field $\mathbf{u}$: in a two-dimensional flow, independent of y (say), $\mathbf{u}=(\partial_x\partial_z\psi,-\partial_x\phi,-\nabla_\perp^2\psi)$ and the velocity components are $\mathbf{u}=[\mathcal{O}(1),\mathcal{O}(E^{-1/3}),\mathcal{O}(E^{-1/3})]$, in agreement with the scaling used in Refs. 4 and 7. Because the reduced equations describe self-consistently the deformation in the mean temperature profile with increasing Rayleigh number, they form a simpler set of equations for studying high Rayleigh number rapidly rotating convection. This is because they can be viewed as the equations describing the dynamics in the bulk. Consequently, the thin (and passive[25]) Ekman boundary lay-

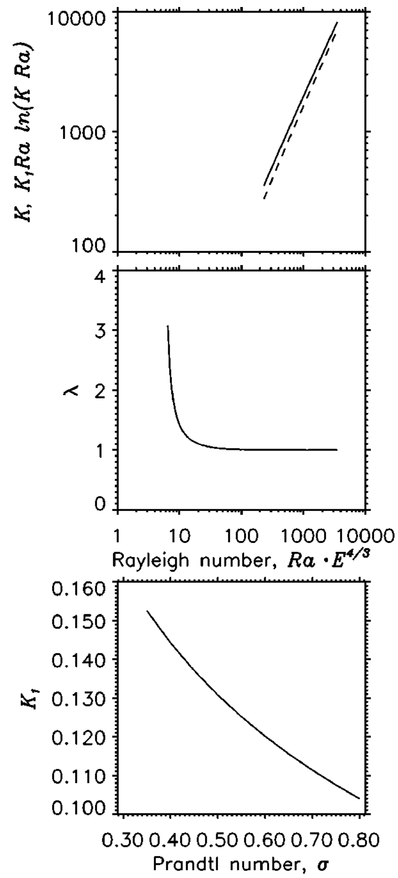

FIG. 12. (a) Comparison of the asymptotic relation (86) for the Nusselt number with exact results obtained from (39) for $\sigma=0.4572$ and $k_c^{(o)}=0.8867$. (b) The eigenvalue $\lambda\equiv\mathrm{Ra}\,K/\rho_0^2$ defined in (78) showing the approach to the asymptotic regime. (c) The prefactor K_1 as a function of σ when $k=k_c^{(o)}$.

ers at the top and bottom are absent, and the resolution requirements substantially reduced. Preliminary simulations of the reduced equations in three dimensions, reported elsewhere,[5] reveal plume structures and vortices extending from top to bottom much as found in three-dimensional simulations of the primitive equations.[6] This approach to describing fully nonlinear rapidly rotating convection will be described in detail elsewhere.

In this paper we have focused on understanding the pattern-forming properties of the reduced equations. Remarkably, a number of patterns can be obtained at arbitrary supercriticality by reformulating the reduced equations as a nonlinear eigenvalue problem. In the case of steady convection, this eigenvalue problem is real and determines the Nusselt number as an eigenvalue for prescribed values of the Rayleigh number. For oscillatory convection, the eigenvalue problem is complex and determines both the time-averaged Nusselt number and the oscillation frequency. In each case the resulting patterns are characterized, at leading order, by a single horizontal wave number, and solve the same eigenvalue problem. Thus no horizontal harmonics are generated in the rapid rotation limit despite the fact that they do become linearly unstable, as happens, for example, at 5.5 Ra 27 Ra_c, and 85 Ra_c in the steady case. The steady patterns for which this is the case include the familiar rolls, as well as squares, hexagons, regular triangles, and a particular rectangular pattern called patchwork quilt. Consequently, all these patterns have the same Nusselt number, i.e., they are equally efficient at transporting heat. Likewise, among the oscillating patterns we identified six (traveling rolls and standing rolls, squares, hexagons, regular triangles, and patchwork quilt) that are characterized by the same time-averaged Nusselt number and identical nonlinear oscillation frequencies. The appearance of these patterns is affected by an unexpected reflection symmetry in vertical planes present in Eqs. (21)–(24) at leading order in the Ekman number. As a result, the leading order equations have the symmetry of a nonrotating system; the handedness expected of rotating systems reappears when the corresponding incompressible velocity field (6) is reconstructed.

We noted that in all cases the patterns guaranteed to exist by abstract theory but inaccessible to the fully nonlinear theory are unstable at onset and hence are not candidates for stable patterns at larger amplitudes. Thus in the rapid rotation limit the large amplitude state is characterized by a competition between a number of computable nearly degenerate states. Because of this near-degeneracy, such competition must occur on a slow time scale. Moreover, the strong influence of the Taylor–Proudman constraint implies that any instabilities lead to states that do not deviate substantially from the computable states. Consequently, we expect the statistical properties of the resulting ''turbulent'' state to be largely independent of which of the competing states is actually present, although distinction between steady, and traveling or standing patterns is necessary. Studies of two-dimensional fully nonlinear convection on an f-plane support this picture and yield semianalytical correlations that are in good quantitative agreement with direct numerical simulations in three dimensions.[25] The slow evolution envisaged above may be viewed as a drift along a manifold of nearly degenerate states. This drift may be due to Küppers–Lortz instabilities whose growth rate is suppressed by the extra reflection symmetry present in the leading order reduced equations. Thus Küppers–Lortz instabilities, like other instabilities, are a consequence of subdominant terms only, and for some patterns (such as squares) may be absent altogether.[11] It is for this reason that we did not consider patterns on the rhombic lattice. General rectangular planforms were also omitted because these result in anisotropic patterns.

The solutions mentioned above are fully nonlinear despite their simple structure in the horizontal. Consequently, the asymptotic limit explored here provides an important instance in which the planform approach of Gough, Spiegel, and Toomre[26–28] to fully nonlinear convection becomes exact. However, not all solutions can be found using this approach, even in the rapid rotation limit. We identified the general conditions for the applicability of the planform approach to the fully nonlinear problem, and determined those solutions for which it failed in the weakly nonlinear regime using center manifold reduction. This reduction in turn identified the likely candidates for stability. Complete stability properties could not be given, however, because of the presence of zero eigenvalues that are not forced by symmetry. The presence of these eigenvalues, which are[7] $\mathcal{O}(E^{4/3})$, indicates that higher order terms in the Ekman number do play an important role in pattern selection; these effects are absent from our reduced equations. Additional effects, such as spatial modulation on $\mathcal{O}(1)$ scales in the original x,y variables, can also be included.[7]

ACKNOWLEDGMENTS

This work was supported by NASA under SR&T Grant No. NAG5-4918 (K.J.) and the Department of Energy under Grant No. DE-FG03-95ER-25251 (E.K.). The authors wish to thank Dr. S. Tobias and Dr. J. Werne for many helpful discussions.

[1]S. Chandrasekhar, *Hydrodynamic and Hydromagnetic Stability* (Oxford University Press, New York, 1961).
[2]G. Veronis, ''Cellular convection with finite amplitude in a rotating fluid,'' J. Fluid Mech. **5**, 401 (1959).
[3]W. Arter [Phys. Lett. **97A**, 171 (1983)] shows that even weakly nonlinear square pattern convection can have chaotic streamlines.
[4]A. P. Bassom and K. Zhang, ''Strongly nonlinear convection cells in a rapidly rotating fluid layer,'' Geophys. Astrophys. Fluid Dyn. **76**, 223 (1994).
[5]K. Julien, E. Knobloch, and J. Werne, ''A new class of equations for rotationally constrained flows,'' Theor. Comput. Fluid Dyn. **11**, 251 (1998).
[6]K. Julien, S. Legg, J. McWilliams, and J. Werne, ''Rapidly rotating turbulent Rayleigh-Bénard convection,'' J. Fluid Mech. **322**, 243 (1996).
[7]K. Julien and E. Knobloch, ''Fully nonlinear oscillatory convection in a rotating layer,'' Phys. Fluids **9**, 1906 (1997).
[8]T. Clune and E. Knobloch, ''Pattern selection in rotating convection with experimental boundary conditions,'' Phys. Rev. E **47**, 2536 (1993).
[9]D. R. Ohlsen, J. E. Hart, and S. Kittelman, ''Laboratory experiments on rotating turbulent convection,'' Am. Met. Soc. Tenth Conf. on Atmospheric and Oceanic Waves and Stability (1995), preprints, p. 255.
[10]S. Sakai, ''The horizontal scale of rotating convection in the geostrophic regime,'' J. Fluid Mech. **333**, 85 (1997).

[11]H. F. Goldstein, E. Knobloch, and M. Silber, ''Planform selection in rotating convection,'' Phys. Fluids A **2**, 625 (1990).
[12]E. Knobloch and M. Silber, ''Hopf bifurcation with $Z_4 \times T^2$ symmetry,'' in *Bifurcation and Symmetry*, edited by E. Allgower, K. Böhmer, and M. Golubitsky (Birkhäuser, Basel, 1992), pp. 241–252.
[13]To the authors' knowledge, only the coefficients *a, b* have been calculated for rotating convection at finite Ta. See E. Knobloch and M. Silber, ''Travelling wave convection in a rotating layer,'' Geophys. Astrophys. Fluid Dyn. **51**, 195 (1990), and Ref. 8.
[14]M. Silber and E. Knobloch, ''Hopf bifurcation on a square lattice,'' Nonlinearity **4**, 1063 (1991).
[15]E. Knobloch and M. Silber, ''Oscillatory convection in a rotating layer,'' Physica D **63**, 213 (1993).
[16]E. Knobloch, ''On the degenerate Hopf bifurcation with O(2) symmetry,'' Contemp. Math. **56**, 193 (1986).
[17]E. Knobloch, ''Symmetry and instability in rotating hydrodynamic and magnetohydrodynamic flows,'' Phys. Fluids **8**, 1446 (1996); A. M. Rucklidge and M. Silber, ''Bifurcations of periodic orbits with spatio-temporal symmetries,'' Nonlinearity **11**, 1435 (1998).
[18]P. Henrici, *Discrete Variable Methods in Ordinary Differential Equations* (Wiley, New York, 1962).
[19]J. R. Cash and A. Singhal, ''High order method for the numerical solution of two-point boundary value problems,'' B.I.T. **22**, 184 (1982).
[20]E. Knobloch, A. Deane, J. Toomre, and D. R. Moore, ''Doubly diffusive waves,'' Contemp. Math. **56**, 203 (1986).
[21]M. Golubitsky, J. W. Swift, and E. Knobloch, ''Symmetries and pattern selection in Rayleigh-Bénard convection,'' Physica D **10**, 249 (1984).
[22]H. F. Goldstein, E. Knobloch, and M. Silber, ''Planform selection in rotating convection: Hexagonal symmetry,'' Phys. Rev. A **46**, 4755 (1992).
[23]M. Roberts, J. W. Swift, and D. H. Wagner, ''The Hopf bifurcation on a hexagonal lattice,'' Contemp. Math. **56**, 283 (1986).
[24]L. N. Howard, ''Heat transport by turbulent convection,'' J. Fluid Mech. **17**, 405 (1963).
[25]K. Julien and E. Knobloch, ''Strongly nonlinear convection cells in a rapidly rotating fluid layer: The tilted *f*-plane,'' J. Fluid Mech. **360**, 141 (1998).
[26]D. O. Gough, E. A. Spiegel, and J. Toomre, ''Modal equations for cellular convection,'' J. Fluid Mech. **68**, 695 (1975).
[27]L. Baker and E. A. Spiegel, ''Modal analysis of convection in a rotating fluid,'' J. Atmos. Sci. **32**, 1909 (1975).
[28]J. Toomre, D. O. Gough, and E. A. Spiegel, ''Numerical solutions of single-mode convection equations,'' J. Fluid Mech. **79**, 1 (1977).